

Numerical Simulation of the Flooding Process of a Compartment with Baffles by MPS Method

Jialin Wu¹, Congyi Huang², Decheng Wan^{2*}

¹ Shanghai Academy of Spaceflight Technology, Shanghai, China

² Computational Marine Hydrodynamics Lab (CMHL), School of Naval Architecture, Ocean and Civil Engineering, Shanghai Jiao Tong University, Shanghai, China

*Corresponding Author

ABSTRACT

The flooding of damaged tank, whether in maritime vessels or industrial settings, poses significant challenges to safety, stability, and structural integrity. Understanding the dynamics of compartment flooding is crucial for mitigating risks and improving design strategies. In this paper, the flooding process of a damaged tank with a baffle is simulated by our in-house MPS (Moving Particle Semi-implicit method) solver MLParticle-SJTU. As a meshless method, MPS method has advantages in simulating strong nonlinear phenomena with large deformation of free surfaces. First, the accuracy of the solver is validated through case simulated by three different numerical methods. Subsequently, the flooding process of compartments equipped with either a horizontal baffle or a vertical baffle is simulated separately. The position of the baffle is varied in horizontal or vertical direction to analyze impacts on the tank flooding process.

KEY WORDS: MPS method, free surface flow, MLParticle-SJTU solver, damaged tank flooding

INTRODUCTION

With the rapid expansion of sea transportation, maritime accidents have become increasingly prevalent. Consequently, understanding the intricate interplay between fluid behavior and structural response during flooding events is essential for developing effective mitigation strategies and enhancing design resilience.

In recent years, numerical methods have become indispensable tools for simulating complex fluid-structure interactions inherent in compartment flooding scenarios. In this regard, the meshless method stands out as a meshless approach with Lagrangian properties, enabling accurate tracking of particle motion and precise representation of free surface phenomena. Consequently, the meshless method has gained widespread adoption in addressing problems characterized by substantial free surface deformations in recent years. Currently, the more prevalent mesh-free particle methods primarily include Smoothed Particle Hydrodynamics (SPH), Particle Finite Element Method (PFEM), and Moving Particle Semi-implicit (MPS) methods. Compared to SPH and PFEM, the MPS method employs a semi-implicit approach to address the pressure term,

resulting in a more stable pressure resolution.

Numerous studies have explored the behavior of damaged compartments employing meshless methods. For instance, Cao et al. (2018) employed a multiphase Smoothed Particle Hydrodynamics (SPH) model to simulate the flooding process of a breached hull while accounting for air effects. González et al. (2003) utilized the SPH method to predict the dynamic responses of damaged Roll-On/Roll-Off (RO-RO) vessels and the occurrence of greenwater events. Touzé et al. (2010) harnessed the SPH method to predict water inflow during ship collisions in waves. Shen & Vassalos (2009) simulated the flooding process of a damaged compartment under rolling and heave motion using the SPH method. Zhang et al. (2013) applied three-dimensional SPH modeling to simulate the flooding and sinking process of a ship model damaged on its side. Ming et al. (2018) conducted an investigation into the flooding process of a damaged compartment in transverse regular waves, employing the Weakly Compressible Smooth Particle Hydrodynamics (WCSPH) method. Zhang et al. (2020) further examined the water ingress process of two-dimensional damaged compartments and analyzed the influence of opening and baffle positions on the inflow dynamics.

Our research group has independently developed the MPS-based solver MLParticle-SJTU, which has been applied to simulate various intense free-surface flows, such as dam break problems (Chen et al. 2019, Zhang et al. 2022), water entry problems (Zha et al. 2022, Huang et al. 2022), liquid sloshing problems (Zhang et al. 2022, Huang et al. 2023) and fluid structure interaction problems (Xie et al. 2022, Zhang et al. 2022). In this paper, the flooding process of a two-dimensional rectangular tank with a baffle is simulated by MLParticle-SJTU solver. Initially, the accuracy and stability of the solver are validated by comparing the results of tank's vertical acceleration and free surface shape with the results obtained by Shen et al. (2009) using VOF and SPH method. Subsequently, the flooding process of the two-dimensional tank with a horizontal or vertical baffle is simulated. By varying the positions of the horizontal or the vertical baffles, we analyze the impact of the baffle positioning on the flooding process of the damaged tank.

NUMERICAL METHOD

The MPS method is a meshless particle method based on the Lagrange

representation method. The computational domain is represented by discrete particles. These particles are not connected by grids or nodes, but carry physical quantities such as mass, velocity and acceleration separately. The flow field is controlled by establishing the governing equation.

Governing equations

The governing equations include the continuity equation and the momentum equation. The governing equation for viscous incompressible fluid can be written as:

$$\frac{1}{\rho} \frac{D\rho}{Dt} = -\nabla \cdot \mathbf{V} = 0 \quad (1)$$

$$\frac{D\mathbf{V}}{Dt} = -\frac{1}{\rho} \nabla P + \nu \nabla^2 \mathbf{V} + \mathbf{g} \quad (2)$$

where ρ is fluid density, \mathbf{V} is velocity vector, P presents pressure, ν is kinematic viscosity, \mathbf{g} is gravitational acceleration vector, t indicates time.

Discretization of the governing equations

In the MPS method, the computational domain is composed of discrete particles. Therefore, the governing equations need to be discretized.

Kernel function

In the MPS method, the interaction between particles is realized by the kernel function, which can be written as:

$$W(r) = \begin{cases} \frac{r_e}{0.85r + 0.15r_e} - 1 & 0 \leq r < r_e \\ 0 & r_e \leq r \end{cases} \quad (3)$$

where $r = |\mathbf{r}_j - \mathbf{r}_i|$ represents the distance between particle i and j , r_e is the influence radius.

Density of the particle number

The particle number density is the sum of kernel functions of all the particles within the influence radius, which can be written as:

$$\langle n \rangle_i = \sum_{j \neq i} W(|\mathbf{r}_j - \mathbf{r}_i|) \quad (4)$$

for incompressible fluid, the particle number density remains constant.

Gradient model

The gradient model is used to discretize the pressure gradient in the governing equation. The expression is:

$$\langle \nabla P \rangle_i = \frac{D}{n^0} \sum_{j \neq i} \frac{P_j + P_i}{|\mathbf{r}_j - \mathbf{r}_i|^2} (\mathbf{r}_j - \mathbf{r}_i) W(|\mathbf{r}_j - \mathbf{r}_i|) \quad (5)$$

where D represents the dimension and n^0 represents the initial particle number density.

Divergence model

Similar to the gradient model, the divergence model is used to discretize the velocity divergence in the governing equation. The expression is:

$$\langle \nabla \cdot \mathbf{V} \rangle_i = \frac{D}{n^0} \sum_{j \neq i} \frac{(\mathbf{V}_j - \mathbf{V}_i) \cdot (\mathbf{r}_j - \mathbf{r}_i)}{|\mathbf{r}_j - \mathbf{r}_i|^2} W(|\mathbf{r}_j - \mathbf{r}_i|) \quad (6)$$

Laplacian model

Laplacian model is used to discretize the second derivative in the governing equation, which can be expressed as:

$$\langle \nabla^2 \phi \rangle_i = \frac{2D}{n^0 \lambda} \sum_{j \neq i} (\phi_j - \phi_i) W(|\mathbf{r}_j - \mathbf{r}_i|) \quad (7)$$

where λ represents the correction of the error introduced by the kernel function, and it can be written as:

$$\lambda = \frac{\sum_{j \neq i} W(|\mathbf{r}_j - \mathbf{r}_i|) |\mathbf{r}_j - \mathbf{r}_i|^2}{\sum_{j \neq i} W(|\mathbf{r}_j - \mathbf{r}_i|)} \quad (8)$$

Pressure Poisson equation

In the MPS method, the Poisson equation is used to solve the particle pressure. The incompressibility of fluid is determined by divergence-free condition and constant particle number density condition. The Poisson equation adopted in this paper is as follows:

$$\langle \nabla^2 P^{k+1} \rangle_i = (1 - \gamma) \frac{\rho}{\Delta t} \nabla \cdot \mathbf{V}_i^* - \gamma \frac{\rho}{\Delta t^2} \frac{\langle n^k \rangle_i - n^0}{n^0} \quad (9)$$

where superscripts k and $k+1$ represent k and $k+1$ time steps. γ is a variable parameter, representing the proportion of particle number density in the source term of Poisson equation. In the original MPS method, the incompressibility of viscous fluids is represented by maintaining a constant particle number density, with the source term of the Poisson pressure equation being solely composed of the particle number density term. Subsequently, Tanaka and Masunaga (2010), drawing inspiration from mesh-based methods where fluid incompressibility is ensured by setting the velocity divergence to zero everywhere, proposed the mixed-source term Poisson pressure equation adopted in this paper. Building on this foundation, Lee and others(2011), established the range for the parameter as [0.01, 0.05] through a series of numerical experiments. The choice of $\gamma = 0.01$ in this paper is based on empirical evidence from previous work, ensuring that while a stable pressure field is solved for, both volume conservation and particle number conservation are maintained.

Detection of free surface particles

When solving the Poisson's pressure equation, it is very important to determine whether a particle is located on a free surface. The number density of particles can be used to determine whether a particle is on a free surface in MPS method. When $\langle n \rangle_i < 0.8n^0$, the particle is considered to be on a free surface. When $\langle n \rangle_i > 0.97n^0$, the particles are thought to be inside the fluid. For particles with particle number density between 0.8 and 0.97, it's difficult to tell whether the particle is on the free surface or inside the fluid. Khayyer and Gotoh(2009) first proposed the criterion which simply based on the fact that for a free-surface particle, the distribution of neighboring particles is asymmetric. In this paper, the vector function \mathbf{F} presented by Zhang et al (2014) is introduced, as follows:

$$\langle \mathbf{F} \rangle_i = \frac{D}{n^0} \sum_{j \neq i} \frac{(\mathbf{r}_i - \mathbf{r}_j)}{|\mathbf{r}_i - \mathbf{r}_j|} W(|\mathbf{r}_i - \mathbf{r}_j|) \quad (10)$$

If $\langle |\mathbf{F}| \rangle_i > 0.9|\mathbf{F}|^0$, the particle i will be considered to be on a free surface. $|\mathbf{F}|^0$ stands for $|\mathbf{F}|$ at the initial time of the free surface particle.

NUMERICAL SIMULATIONS

In this section, the inner solver MLParticle-SJTU is used to simulate the flooding process of a two-dimensional damaged cabin. Firstly, the stability and accuracy of the solver are verified by simulating the water inlet process of two-dimensional square cabin with side opening, and compare the results obtained by VOF method and SPH method.

Numerical validation

As depicted in Fig. 1, the model is a square tank with each side measuring 0.1 meters and featuring an opening positioned 0.02 meters above the side. Additional specific parameters of the model are detailed in Table 1. This study simulates the water inlet process of the model. The computational domain extends to 0.4 meters in length and 0.3 meters in height. The initial particle spacing is set at 0.05 mm, with a time step of 0.001 seconds. The fluid density is 1000 kg/m^3 , and the kinematic viscosity coefficient is $1 \times 10^{-6} \text{ m}^2/\text{s}$. The simulation involves a total of 88,613 particles, comprising 72,375 fluid particles and 3,350 boundary particles.

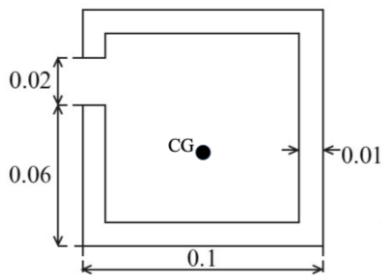


Fig. 1. Schematic diagram of the computational model

Table 1. Model scale parameters	
parameter	value
Weight(kg)	7.5
Moment of inertia with respect to Z axis($\text{kg} \cdot \text{m}^2$)	0.075
Length(m)	0.1
Height(m)	0.1
Coordinates of gravity center(m)	(0.2, 0.175)
Thickness(m)	0.01
ship draft(m)	0.075

The simulation outcomes of the MPS method are juxtaposed with those derived from the VOF and SPH methods by Shen et al. (2009), as illustrated in Fig. 2. This figure presents the fluid distribution and hull motion during the simulation. For the SPH and MPS methods, the computational domain contains only fluid particles, with red (SPH) and yellow (MPS) indicating the fluid particles, and the deep blue border representing the liquid tank. For the VOF method, since the simulation of free surface flows using the VOF method involves two-phase flow, in the results of the VOF method, the red part represents the fluid, the blue part represents the gas, and the white border indicates the liquid tank. In Figure 2, the images in the three rows from top to bottom respectively show the results obtained by the VOF, SPH, and MPS methods. From left to right, each column of images illustrates the flow field distribution and liquid tank configuration corresponding to 0.1s, 0.2s, 0.3s, and 0.4s. As evident from Fig.2, the results acquired from these three methods exhibit a high degree of concordance. At 0.1s, fluid ingress into the cabin is initiated. By 0.2s, the fluid reaches the bottom of the sheltered area. At

the 0.3s interval, fluid accumulation is observed on the right side of the bottom, exerting an impact on the right bulkhead. By 0.4s, fluid begins to pool on both sides, with a noticeably greater volume on the right side. The MPS simulation results align well with existing data, accurately reflecting both the cabin motion pattern and the fluid distribution within the cabin.

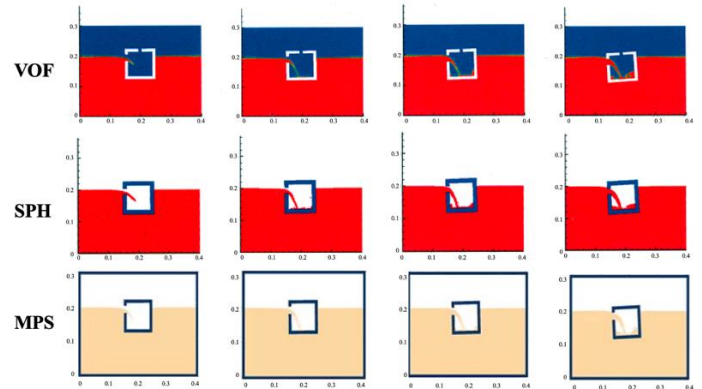


Fig. 2. From left to right: 0.1s, 0.2s, 0.3s, 0.4s, From top to bottom: VOF, SPH, MPS

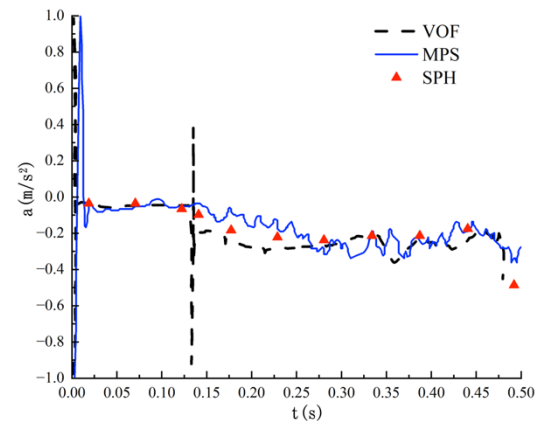


Fig. 3. Comparison of horizontal acceleration of VOF and SPH (Shen et al. 2009) and MPS

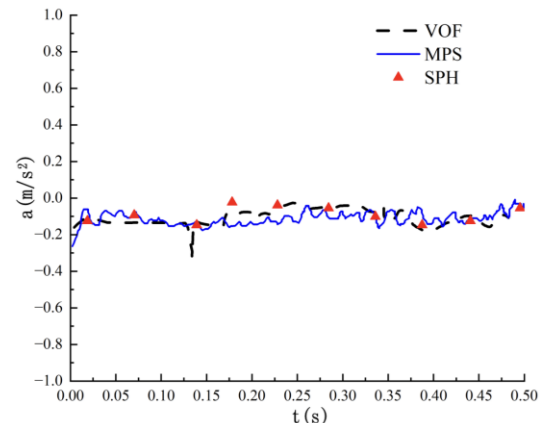


Fig. 4. Comparison of vertical acceleration of VOF and SPH (Shen et al. 2009) and MPS

Figs. 3 and 4 depict the comparison of horizontal and vertical accelerations at the center of gravity, respectively, between the MPS and SPH methods. The horizontal acceleration, initially characterized by

significant oscillations, gradually stabilizes to a smaller amplitude, closely aligning with the results obtained from the SPH method. In contrast, the vertical acceleration demonstrates oscillations around -0.1m/s^2 , with an amplitude substantially smaller than that observed in the vertical direction. This trend also shows a good correlation with the SPH method outcomes. These analyses comprehensively demonstrate that the MlParticle-SJTU solver is capable of effectively simulating the flooding process in a damaged hull, capturing both the horizontal and vertical dynamic responses accurately.

Simulation of flooding process in a tank with a horizontal baffle

In this section, the flooding process of a tank with a horizontal baffle is simulated. A comparative analysis is conducted to investigate the influence of the baffle's position. The rectangular liquid compartments with the baffle at different positions are illustrated in Fig. 5. The velocity distribution of the flow field during the flooding process simulated by MPS method is depicted in Fig. 6. The displacements along the horizontal and vertical directions of the compartment, as well as the rotational angles are recorded. The time history curves are plotted accordingly, as shown in Figs. 7, 8, and 9.

Fig. 6 illustrates the velocity distribution at four distinct time points, providing a clear visualization of the fluid dynamics within the compartment. At $t=0.3\text{s}$, the fluid gradually enters the chamber, predominantly accumulating on the horizontal baffle. The uneven distribution of fluid, with less accumulating at lower positions on the baffle, translates into a non-uniform distribution of force exerted by the fluid on the compartment's walls. According to the principles of torque, $\tau = r \times F$, where τ is torque, r is the distance from the pivot point, and F is the force applied, the reduced accumulation at lower positions implies a reduction in the magnitude of the force vector component perpendicular to the lever arm (baffle). Consequently, this leads to a decreased torque exerted on the compartment, resulting in a smaller rotation angle, as shown in Fig. 9.

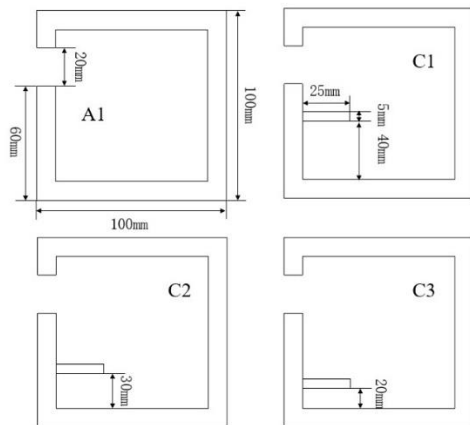


Fig. 5. Schematic diagram of the damaged cabin with a horizontal baffle

As the compartment begins to rotate, the dynamic interaction between the fluid and the compartment's structure evolves. The gravitational force acting on the fluid causes it to pool at the compartment's lowest point, initially in the lower right corner. The phenomenon of inflow trajectory reversal around $t=0.6\text{s}$ can be explained through the concept of fluid pressure and hydrostatic equilibrium. As the fluid depth increases at the bottom, the pressure at the bottom of the compartment increases, which can alter the flow direction of the incoming fluid due to the differences in pressure gradients.

The mention of the C3 model experiencing a consistent inflow reversal phenomenon due to the lower placement of the baffle, compared to the C2 model, underlines the significant impact of structural differences on fluid dynamics. The placement of the baffle affects the flow pattern and the distribution of forces within the compartment. By $t=0.8\text{s}$, when the compartment becomes fully submerged, the system transitions to a new state where buoyancy forces become dominant. According to Archimedes' principle, the upward buoyancy force experienced by the compartment is equal to the weight of the fluid displaced by the compartment. This marks a critical phase in the analysis of fluid dynamics, as the interaction between the fluid's kinetic energy, the compartment's structure, and external forces such as gravity and buoyancy define the subsequent motion and stability of the system.

From Figs. 7 and 8, it is evident that from the initiation of water ingress into the compartment until complete submergence, the presence of the horizontal baffle has minimal influence on the horizontal and vertical motions of the compartment. However, for the C1 model, the temporal curves of the horizontal and vertical displacements of the compartment nearly overlap with those of the un-baffled compartment. This may be attributed to the fact that until the compartment begins rotation, the vertical forces acting on the compartment are identical, regardless of whether the liquid accumulates on the baffle or at the bottom of the compartment. As the compartment begins to rotate and inflow reversal occurs, the baffle in the C1 model barely affects the development of the reverse flow in the flow field. In contrast, for the C2 and C3 models, the presence of the baffle inhibits the development of the reverse flow, altering the fluid's trajectory and consequently affecting the forces acting on the compartment in the X and Y directions, restraining its displacement. Regarding the rotational motion of the compartment.

Fig. 9 illustrates that the presence of the baffle in the C1 model not only fails to inhibit the rotation but exacerbates it. This is because the initial accumulation of liquid on the baffle increases the bending moment applied to the compartment, accelerating its instability in the rotational direction. In contrast, for the C2 and C3 models, where the baffle is positioned lower, there is no initial accumulation of liquid above the baffle, and during the gradual accumulation of liquid, the presence of the baffle effectively inhibits the development of inflow reversal, thereby providing better restraint on the rotational motion of the compartment. Moreover, in the C3 model, where the baffle position is lower, the inhibitory effect on rotation is more pronounced.

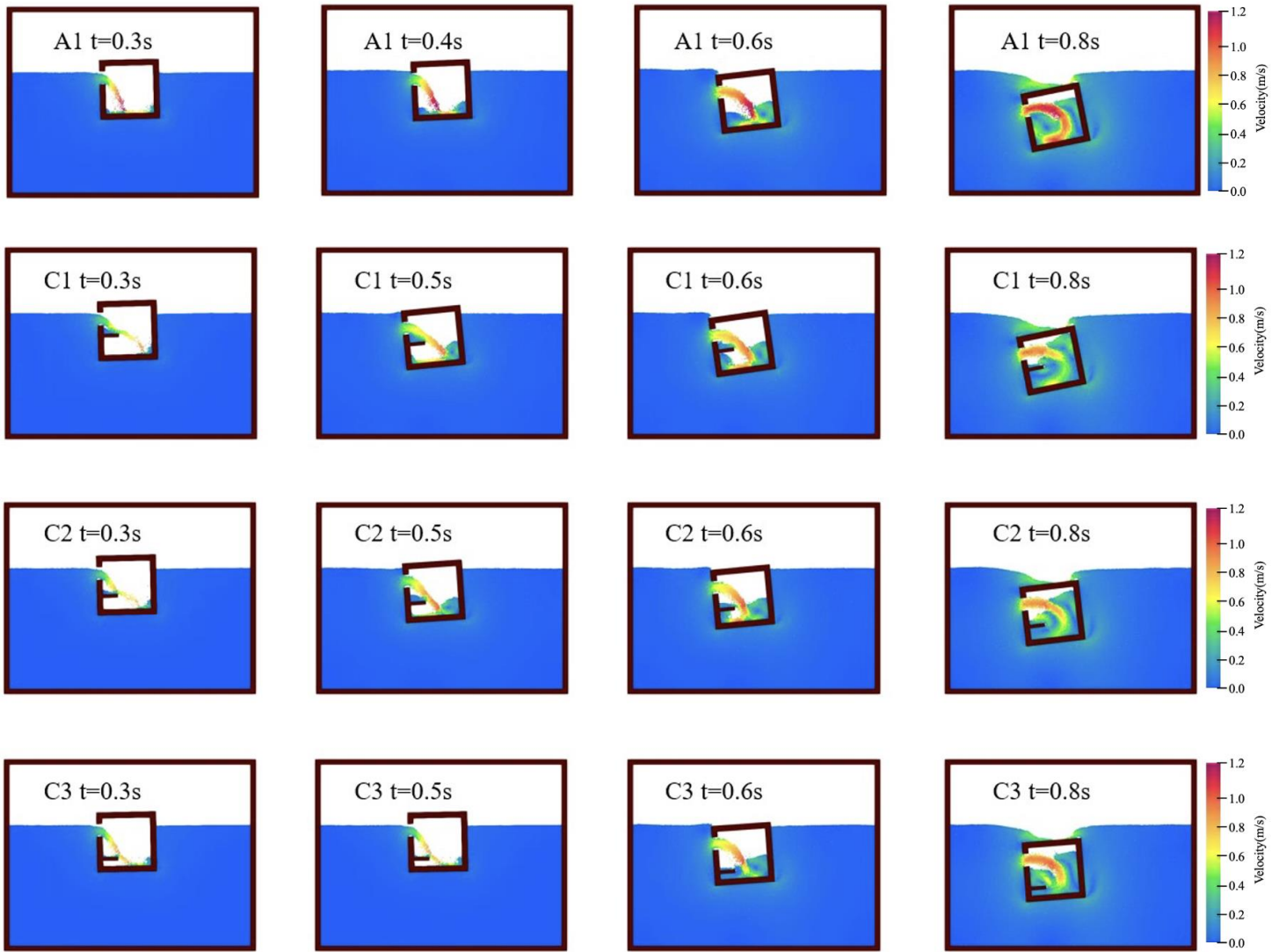


Fig. 6. Schematic diagram of the velocity distribution during the flooding process of a damaged compartment with a horizontal baffle

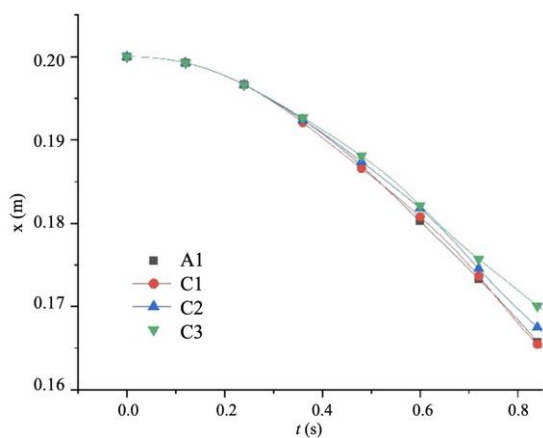


Fig. 7. Time history curves of horizontal displacement of the liquid compartment with a horizontal baffle at different positions

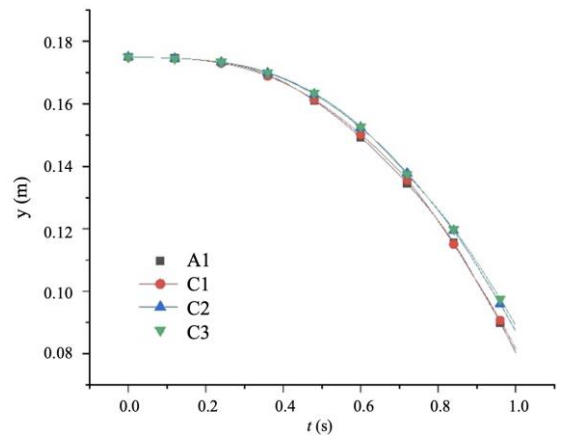


Fig. 8. Time history curves of vertical displacement of the liquid compartment with a horizontal baffle at different positions

Simulation of flooding process in a tank with a vertical baffle

In this section, the simulation focuses on the flooding process within a

compartment featuring a vertical baffle. This study conducts a comparative analysis to elucidate the impact of the baffle's position on the dynamics of the flooding process. Fig. 10 presents the configuration of the rectangular liquid compartment with the integrated baffle. In the simulations presented in this paper, changes in the distribution of water within the tank due to the alteration of the baffle's position are considered exclusively. This paper focuses solely on the variations in the tank's movement prompted by the liquid's distribution, while disregarding the impact of the baffle's position on the tank's motion. Consequently, it is assumed that the mass and the center of gravity of the tank remain constant across the four cases depicted in Fig. 10. The simulated velocity distribution within the flow field during the flooding event is showcased in Fig. 11. This research meticulously records the compartment's displacements in both horizontal and vertical directions, along with its in-plane rotational angles. The temporal evolution of these parameters is plotted and can be observed in Figs. 12, 13, and 14, offering insight into the progression of the flooding process.

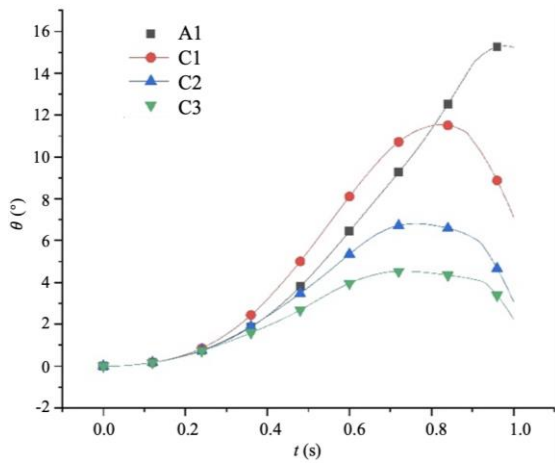


Fig. 9. Time history curves of the rotational angle of the liquid compartment with a horizontal baffle at different positions

It can be seen from Fig.11 that at $t=0.2s$, the liquid begins to ingress into the compartment through the side opening, subsequently accumulating at the bottom. In D2 and D3, the liquid predominantly gathers on one side of the baffle. In contrast, in D1, the baffle effectively bifurcates the liquid at its apex, redirecting the flow towards both sides. By $t=0.4s$, as the compartment submerges deeper and the inflow velocity at the entrance intensifies, the angle between the inflow trajectory and the compartment sidewall becomes larger. Concurrently, the compartment starts to exhibit rotational movement. Specifically, in the D1 model, the liquid chiefly accumulates on the baffle's right side. However, in D2 and D3, the predominant liquid accumulation remains on the left side of the baffle. Notably, scenarios D2 and D3 exhibit inflow reversal and surface rolling phenomena. Moreover, in D2, the larger distance between the accumulated liquid's center of mass and the compartment's center of

mass generates a more significant moment, resulting in an increased rotation angle.

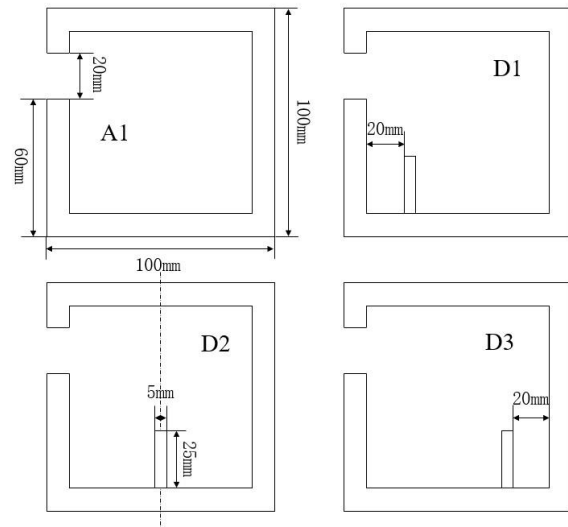


Fig. 10. Schematic diagram of the damaged cabin with a vertical baffle

At $t=0.6s$ in D1, the rotation and inflow velocity amplify, directing the entire inflow to the right side of the baffle, thereby counteracting the initial leftward tilt and maintaining a relatively minor tilt angle. For the D2 model, as the tilt angle augments, the inflow similarly shifts entirely to the baffle's right side, but the asymmetric fluid distribution on either side of the baffle hastens the leftward tilting. In the D3 model, due to the baffle's extreme right positioning, the fluid continues to accumulate predominantly on the left side of the baffle's bottom. By $t=0.7s$, the compartment undergoes complete capsizing. Fig. 11 depicts considerable fragmentation of the free surface within the compartment, phenomena that are challenging to replicate using mesh-based methods. In such complex situations, meshfree methods show their distinct advantages, adeptly handling these intricate fluid dynamics.

It can be seen from Fig.12 that the position of a vertical baffle at the compartment's bottom has a negligible impact on its horizontal motion, but a vertical baffle at the bottom not only fails to mitigate vertical displacement but rather amplifies it. In conjunction with insights from Fig. 11, this exacerbation of vertical displacement could be ascribed to the increased tilt angle, which provokes instability and amplifies vertical motion. Fig. 14 shows that in D2 and D3, the vertical baffle escalates the rotational movement and accelerates the onset of capsizing. Conversely, in D1, the judicious placement of the baffle effectively redistributes the fluid at the bottom, thereby curtailing rotational movement and enhancing rotational stability.

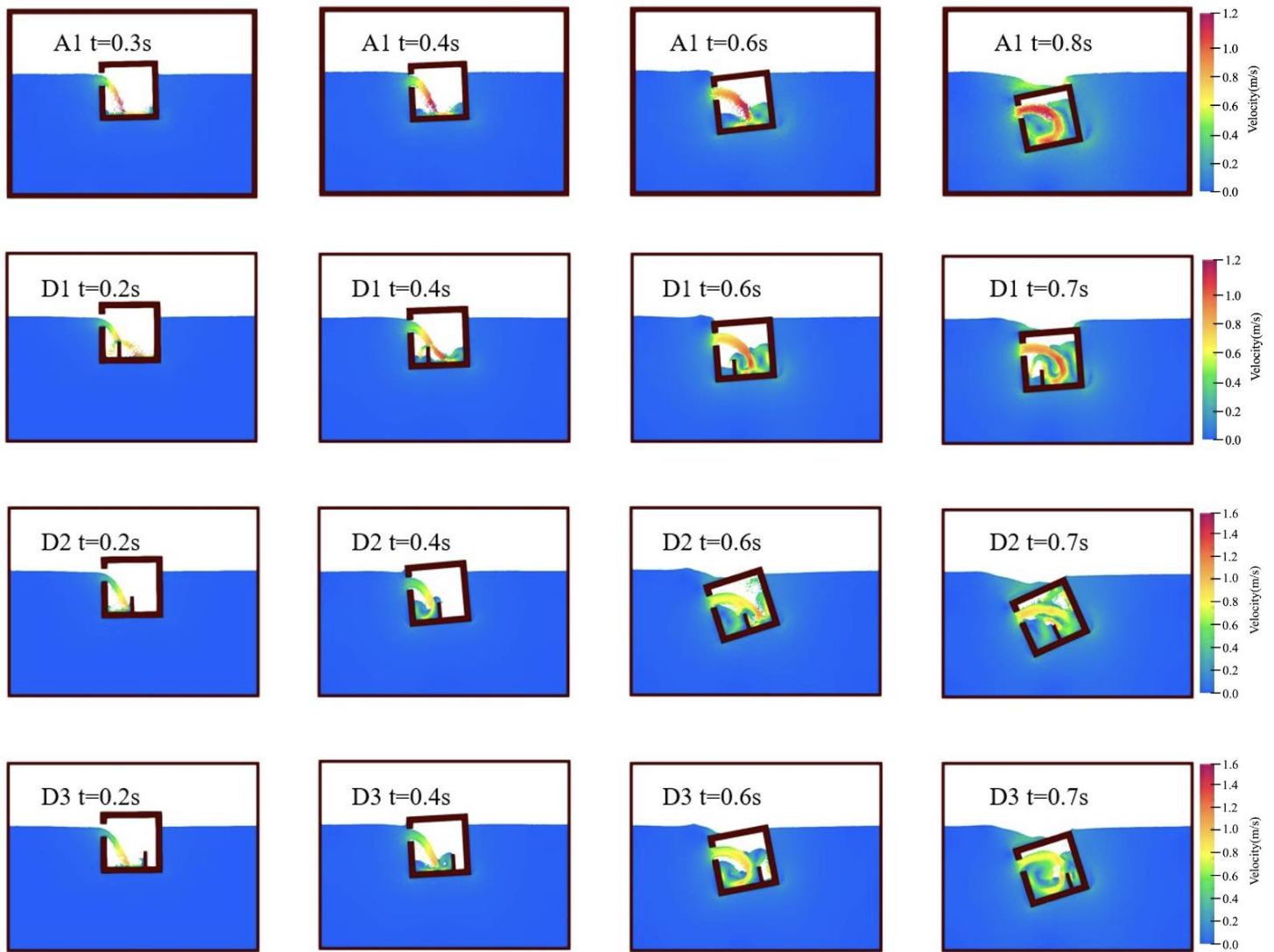


Fig. 11. Schematic diagram of the velocity distribution during the flooding process of a damaged compartment with a vertical baffle

CONCLUSIONS

This paper simulates the flooding process of two-dimensional rectangular compartments equipped with both horizontal and vertical baffles. Initially, the flooding process of a two-dimensional rectangular compartment is simulated, and the results are compared with experimental data and previously published results obtained using the SPH method to validate the accuracy of the solver in simulating such flooding scenarios. Subsequently, the flooding process of compartments equipped with a horizontal and a vertical baffle, respectively, is simulated. The dimensions of the baffles are consistent, but their positions vary. For the horizontal baffle, among the three selected operating conditions, a lower baffle position exhibits better inhibition of the compartment's rotational motion. Conversely, a higher baffle position may exacerbate the compartment's rotational motion. The horizontal and vertical displacements are minimally influenced by the horizontal baffle. Regarding the vertical baffle, among the three scenarios simulated in the paper, placing a vertical baffle accelerates the compartment's vertical displacement. A vertical baffle placed in an appropriate position can suppress the compartment's rotational motion, whereas placing it in an inappropriate position may accelerate the compartment's rotational motion.

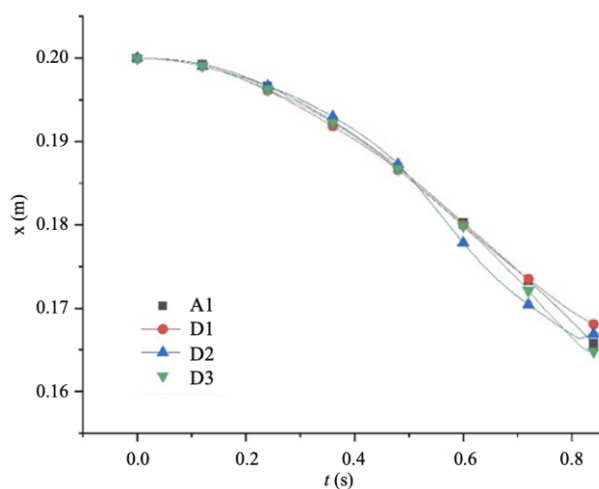


Fig.12 Time history curves of horizontal displacement of the liquid compartment with a vertical baffle at different positions

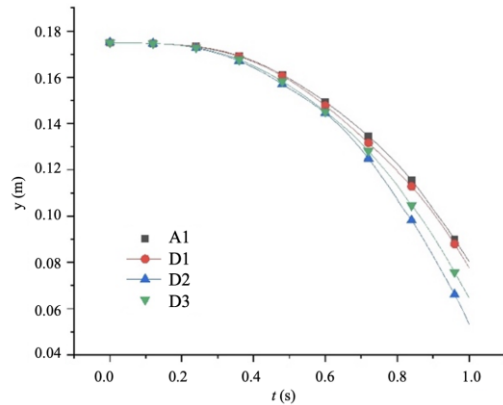


Fig.13 Time history curves of vertical displacement of the liquid compartment with a vertical baffle at different positions

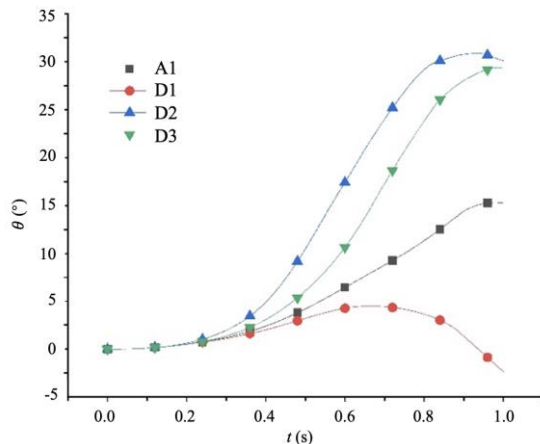


Fig.14 Time history curves of the rotational angle of the liquid compartment with a vertical baffle at different positions

ACKNOWLEDGMENTS

This work is supported by the National Natural Science Foundation of China (52131102), to which the authors are most grateful.

REFERENCES

Cao, XY, Ming, FR, Zhang, AM, Tao, L (2018). "Multi-phase SPH modelling of air effect on the dynamic flooding of a damaged cabin," *Computers & Fluids*, 163: 7-19.

Chen, X, Wan, DC (2019). "Numerical Simulation of Three-Dimensional Violent Free Surface Flows by GPU-Based MPS Method," *International Journal of Computational Methods*, 16(4), 1843012-1-1843012-20.

González, V, Talens, M, Riola, JM, Valle, J, Espin, M (2003). "Numerical prediction of the dynamic behavior of a Ro-Ro ship after a hull side damage," *Proceedings of the 8th International Conference on Stability of Ships and Ocean Vehicles*, Madrid: 215-227.

Huang, CY, Zhang, GY, Wan, DC (2022). "Hydroelastic responses of an elastic cylinder impacting on the free surface by MPS-FEM coupled method," *Acta Mechanica Sinica*, 38, 322057.

Huang, CY, Zhao, WW, Wan, DC(2023). "Numerical simulations of faraday waves in cylindrical and hexagonal tanks based on MPS method," *Journal of Hydrodynamics*, 35(2): 278-286.

Khayyer, A, Gotoh, H and Shao, S (2009). "Enhanced predictions of wave impact pressure by improved incompressible SPH methods," *Applied Ocean Research*, 31(2),111-131.

Lee, BH, Park, JC, Kim, MH, Hwang, SC (2011). "Step-by-step improvement of MPS method in simulating violent free-surface motions and impact-loads," *Computer Methods in Applied Mechanics and Engineering*, 200, 1113-1125.

Ming, FR, Zhang, AM, Cheng, H, Sun, PN (2018). "Numerical simulation of a damaged ship cabin flooding in transversal waves with smoothed particle hydrodynamics method," *Ocean Engineering*, 165: 336-352.

Shen, L, Vassalos, D (2009). "Applications of 3D parallel SPH for sloshing and flooding," *Proceedings of the 10th International Conference on Stability of Ships and Ocean vehicles*, St. Petersburg: 723-732.

Tanaka, M and Masunaga, T (2010). "Stabilization and smoothing of pressure in MPS method by Quasi-Compressibility," *Journal of Computational Physics*, 229(11), 4279-4290.

Touzé, DL, Marsh, A, Oger, G, Guilcher, PM, & Ferrant, P (2010). "SPH simulation of green water and ship flooding scenarios," *Journal of Hydrodynamics*, 22(5), 231-236.

Xie, FZ, Meng, QJ, Wan, DC (2022). "Numerical Simulations of Liquid-Solid Flows in A Vertical Pipe by MPS-DEM Coupling Method," *China Ocean Engineering*, 36: 542-552.

Zha, RS, Zhao, WW, Wan, DC(2022). "Numerical Study on Water Entry of Projectiles with Various Head Shapes by a Multiphase Moving Particle Semi-implicit Method," *International Journal of Offshore and Polar Engineering*, 32(4): 402-410.

Zhang, AM, Cao, XY, Ming, FR, Zhang, ZF (2013). "Investigation on a damaged ship model sinking into water based on three dimensional SPH method," *Applied ocean research*, 42: 24-31.

Zhang, GY, Wu, JX, Sun, Z, Moctar, O, Zong, Z (2020). "Numerically simulated flooding of a freely-floating two-dimensional damaged ship section using an improved MPS method," *Applied Ocean Research*, 101: 102207.

Zhang, GY, Zha, RS, Wan, DC (2022). "MPS-FEM coupled method for 3D dam-break flows with elastic gate structures," *European Journal of Mechanics / B Fluids*, 94: 171-189.

Zhang, GY, Zhao, WW, Wan DC (2022). "Moving Particle Semi-implicit method coupled with Finite Element Method for hydro-elastic responses of floating structures in waves," *European Journal of Mechanics / B Fluids*, 95: 63-82.

Zhang, GY, Zhao, WW, Wan, DC (2022). "Numerical simulations of sloshing waves in vertically excited square tank by improved MPS method," *Journal of Hydrodynamics*, 34(1): 76-84.

Zhang, YL, Wan DC (2018). "MPS-FEM coupled method for sloshing flows in an elastic tank," *Ocean Engineering*, 152, 416-427.

Zhang, YX, Wan, DC, Hino, T (2014a). "Application of MPS method in liquid sloshing," *The China Ocean Engineering*, 32(4): 24-32.

Zhang, YX, Wan, DC, Hino, T (2014b). "Comparative study of MPS method and level-set method for sloshing flows," *Journal of Hydrodynamics*, 26(4): 577-585 .